J Sol-Gel Sci Technol (2008) 47:300–310
DOI 10.1007/s10971-008-1755-7

ORIGINAL PAPER

In situ fluorescence probing of the chemical and structural changes during formation of hexagonal phase cetyltrimethylammonium bromide and lamellar phase CTAB/ Poly(dodecylmethacrylate) sol–gel silica thin films

Michael H. Huang · Hermes M. Soyez · Bruce S. Dunn · Jeffrey I. Zink · Allan Sellinger · C. Jeffrey Brinker

Received: 9 February 2008 / Accepted: 22 April 2008 / Published online: 17 May 2008

Abstract Surfactant-templated mesostructured sol–gel films formed by evaporation induced self assembly (EISA) exhibit highly-ordered hexagonal, lamellar, and cubic structures. The steady-state dip-coating configuration allows both the chemistry and the dynamics of the EISA process to be traced in real time because the steps involved in the formation of the mesostructured material are separated both spatially and temporally in the dip-coating direction. The dynamic processes occurring during film formation can be conveniently monitored by the combination of interferometry and fluorescence spectroscopy of incorporated molecular probes. The selected probes respond to changes in their rotational mobility and the surrounding solvent composition and report these changes through their fluorescence characteristics. By taking in situ fluorescence spectra at various positions within the progressively thinning film, changes in the solvent composition, onset of micelle formation and further organization to the final mesophase structure can be followed. The luminescence of the probe molecule is measured with a spatial resolution of 100 μm. Two categories of surfactant-templated mesostructured sol–gel films were examined. Cetyltrimethylammonium bromide (CTAB) systems assemble into a 2-D hexagonal surfactant/silica mesophase with the surfactant concentration used in this study. CTAB dodecylmethacrylate systems assemble into a lamellar mesophase, which can be further polymerized to form a poly(dodecylmethacrylate)/silica hybrid nanocomposite that mimics nacre. X-ray diffraction patterns, transmission electron microscopy images, and other techniques are used to characterize the final films.

Keywords Thin films · Optical probe · Mesostructure

M. H. Huang · J. I. Zink (✉)
Department of Chemistry and Biochemistry, University of California, Los Angeles, CA 90095, USA
e-mail: zink@chem.ucla.edu

M. H. Huang
Department of Chemistry, National Tsing Hua University, Hsinchu 30013, Taiwan

H. M. Soyez · B. S. Dunn (✉)
Department of Materials Science and Engineering, University of California, Los Angeles, CA 90095, USA
e-mail: bdunn@ucla.edu

A. Sellinger · C. J. Brinker (✉)
The Advanced Materials Laboratory, NSF Center for Micro-Engineered Materials, Sandia National Laboratories and the University of New Mexico, 1001 University Blvd. SE, Albuquerque, NM 87106, USA
e-mail: cjbrink@sandia.gov

1 Introduction

Sol–gel synthesis of silica materials has a long history and has been reviewed extensively [1–4]. Recent developments in the preparation of surfactant-templated mesostructured sol–gel silica materials have extended the morphology from the originally discovered powders, with particle sizes on the order of microns [5, 6], to continuous thin films [7–16]. Mesostructured sol–gel thin films formed by evaporation induced self assembly (EISA) during dip-coating have been made with hexagonal, lamellar, and cubic structures possessing a high degree of long-range order [17, 18].

During dip-coating, when the upward moving flux of the entrained fluid is balanced by evaporation, the dip-coating thickness profile becomes steady. This allows both the chemistry and the dynamics of the assembly process to be traced in real time, because the steps involved in the formation of the mesostructured sol–gel material are separated

both spatially and temporally in the dip-coating direction [19–22]. The starting point of the process is a dilute homogeneous solution containing all of the components that assemble to form the final mesostructured silica film. Micelle and mesophase formation, as well as continued condensation reactions that form silica, occur progressively within the thinning film entrained on the substrate withdrawn at a constant rate from the solution. These processes occur at different heights above the sol and times; the spatial separation allows the various stages of the process to be examined.

To monitor changes in solvent composition and micelle and mesophase formation during dip-coating, luminescent molecules that probe a particular aspect of the film-forming process can be incorporated in the surfactant sol. Luminescent molecules that respond to changes in the solvent composition can interrogate the dynamic changes in the relative amount of water and alcohol that occur in real time during film formation. Other probe molecules can be chosen to probe the rigidity in their immediate environment, and thus interrogate the system in real time concerning formation of micelles. The measurements are non-destructive, and low concentrations of the probe molecules do not perturb the processing dynamics.

The film formation process starts with a solution of the silica precursor (a tetraalkoxy silane), solvent (water and alcohol), surfactant (for surfactant-templated films), and catalyst (HCl). In the dip-coating process, a substrate is slowly withdrawn from the sol reservoir. The moving substrate entrains the sol, forming an initially liquid film. The film thins by solvent evaporation and gravitational draining. When the upward moving flux is balanced by that of the evaporation and gravitational draining, a steady film profile, 1–2 cm in height, is established. The film profile is wedge-shaped until it reaches a final thickness beyond which it is essentially constant [23]. Concurrent with this process is the formation of both silica and micelles and their transformation into the ordered mesostructure. The thickness of the film can be measured optically by using interferometry. By simultaneously combining spectroscopy of the luminescent molecular probes with interferometry, both the dynamic chemical and structural changes that occur during the EISA process can be followed [24–27].

The dynamic properties of particular importance in this study are the changes in film thickness, solvent composition, and micelle formation as a function of time. The thickness is monitored by interferometry. When the substrate is withdrawn from the solution at a constant rate, a steady-state develops in a few seconds in which the film thickness at a given height above the solution remains constant even though the substrate is moving. The interference fringes remain constant in the dynamic system. The film thickness at a given height and thus at a given time in the formation process is measured. The thickness of the film ranges from 150 nm in final dried films to about 3,500 nm near the solution reservoir. Simultaneously, the luminescence of the probe molecule is measured with a spatial resolution of 100 μm (corresponding to a temporal resolution of about 0.1 s at the pull rate of 7 cm/s). The solvent composition is measured by the ratio of the intensities of two fluorescence peaks that is quantitatively related to the alcohol:water ratio. Micelle formation is measured by the fluorescence depolarization of a probe molecule. This measures the hindrance of the probe molecule's motion when it is incorporated in a micelle.

In this paper, we use these optical methods to examine the film formation process of two kinds of dip-coated surfactant-templated sol–gel film systems: hexagonal mesostructured silica films templated by cetyltrimethylammonium bromide (CTAB) and lamellar mesostructured organic–inorganic laminated nanocomposite films templated by CTAB, dodecylmethacrylate (DM) and hexanedioldimethacrylate (HDM). The organic–inorganic nanocomposite structure is intended to mimic nacre, which provides enhanced hardness to the film. Evolution in the solvent composition of control films, made from the same sol but without CTAB, is also studied. We first discuss the evolving EtOH/H_2O solvent composition. Next, we characterize the structure and monitor the formation of CTAB-templated 2-D hexagonal thin film mesophases. Finally, we report the synthesis, structural characterization, and dynamic processes of lamellar mesostructured organic–inorganic laminated nanocomposite films.

2 Experimental section

2.1 Materials preparation and film characterization

Films containing CTAB that were prepared through addition of 2.5 wt% CTAB to the parent sol form a 2-D hexagonal mesophase with cylindrical micelles oriented parallel to the substrate surface [19]. Spatially resolved fluorescence depolarization experiments using a hydrophobic dye 2-*p*-toluidinyl naphthalene-6-sulphonate (2,6-TNS, Aldrich) were performed to identify micelle formation during film deposition. A stock solution was prepared by refluxing tetraethoxysilane (TEOS) (Aldrich), ethanol, water, and HCl (mole ratio: 1:3.8:1:5 $\times$ 10^{-5}) at 60°C for 90 min. Typically 0.3 ml of deionized water and 0.9 ml of 0.07 N HCl were added to 7.5 ml of the stock solution increasing the HCl concentration to 7.34 mM. The sol was stirred for 15 min and then aged for another 15 min at room temperature for both steps, followed by dilution with two equivalents of ethanol. 0.056 M (2.5 wt%) of CTAB was added to the sol. The final reactant proportions were 1:22.3:5.1:0.004:0.091 TEOS/ethanol/H_2O/HCl/CTAB. 1×10^{-4} mol 2,6-TNS

(Aldrich) was then added to the sol. CTAB was omitted from the sol in the control experiments. The films were formed on silicon substrates by dip-coating at a withdrawal speed of ~7 cm/min.

The same sol used in the control experiments was used to monitor evolution in the solvent composition during film deposition. The probe used here is pyranine (trisodium 8-hydroxy-1,3,6-pyrenetrisulfonate). 1×10^{-4} mol pyranine (Sigma Chemical Co.) was added to the sol. A film drawing speed of ~5 cm/min was used.

Organic–inorganic poly(dodecylmethacrylate) (PDM)/silica nanocomposite coatings have hard/soft laminated structures with analogy to nacre [28]. In situ fluorescence depolarization measurements of a polymerizable probe 1-pyrenylmethyl methacrylate (1-PMM) were used to monitor micelle and mesophase formation. Precursor solutions were prepared by addition of organic monomer, crosslinker, initiator, and an unsaturated alkyltrialkoxysilane to the stock solution used previously. Coupling agent [7-octenyltrimethoxysilane (OTS)] was added to this sol followed by CTAB (3.5 wt%), monomer (DM), crosslinker (HDM), and photo-initiator [ultraviolet, benzoin methyl ether (BME)]. The final reactant mole ratio was 1:22.3:5.1:0.004:0.21:0.16:0.02:0.08:0.02 TEOS/EtOH/H_2O/HCl/CTAB/DM/HDM/OTS/BME. Finally 1×10^{-4} mol of 1-PMM (Polysciences, Inc.) was then added to the sol. Two other solutions were prepared for the control experiments. In one solution only 3.5 wt% CTAB was added to the ethanol-diluted sol. In the other solution 3.5 wt% CTAB and about the same amount of the coupling agent OTS as that used in the standard sol were added to the ethanol-diluted sol. The films were withdrawn at a speed of ~7 cm/min.

Dip-coating was performed using the apparatus described previously [23]. This approach uses hydraulic motion to produce a steady and vibration-free withdrawal. Polished Si (100) substrates (9 cm × 1 cm × 1 mm) were cleaned with Nochromix (Godax Laboratories Inc.) and then rinsed with and stored in deionized water prior to use. These substrates were connected, through a ribbon, to a weighted float in a cylindrical water tank whose drainage was controlled by a flow valve. On top of the sol reservoir a transparent Pyrex cover was placed to reduce air convection and to slow the evaporation rate. Convection-free drying was found to be critical to obtaining high optical quality films. A small opening on the Pyrex cover allows the passage for the excitation laser and collection of the probe emission. Film pulling speed was ~7 cm/min (except for the pyranine experiments). Steady state conditions and fringe patterns were established within 15 s at this rate. After film deposition, thicknesses of some dried films were measured by surface profilometry (Alpha-Step 200, Tencor Instrument).

The structure of the final mesostructured films were characterized with X-ray diffraction (XRD) and transmission electron microscopy (TEM) imaging. Calcination of the films at 400°C for 4 h removes the surfactant. XRD patterns taken before and after calcination often assist in the determination of the kinds of mesostructures present in the films. Color changes are often observed in the calcined films, indicating the shrinkage of the films through the removal of surfactant and continued condensation reactions.

2.2 Probe molecules

The fluorescent molecular probe molecules used in this work were pyranine (trisodium 8-hydroxy-1,3,6-pyrenetrisulfonate) (I), 2,6-TNS (2-*p*-toluidinyl naphthalene-6-sulphonate) (II), and 1-PMM (III). Their structures are shown in Fig. 1.

Pyranine is sensitive to proton transfer in the medium surrounding the molecule [29], and was used to monitor and quantify the water:alcohol ratio in the non-surfactant sol during film deposition. The protonated form has an emission maximum at 430 nm (e.g., in ethanol) and the deprotonated form has a maximum at 510 nm (e.g., in water) [30–32]. Pyranine has been used to monitor both the alcohol/water ratios in sol–gel films [23] and pH [29, 32, 33]. It has also been successfully used to measure the alcohol/water content of aluminosilicate gels during the sol–gel-xerogel transformation and to study the effect of pH on water consumption during gelation of a silica system [30, 34].

The probe 2,6-TNS was used to follow the formation of both the micelles and the hexagonal mesophase (This probe has also been used in the study of hydrophobic regions of proteins [35]). Micelles form when the surfactant concentration in the evaporating film exceeds the critical micelle concentration (CMC). Incorporation of 2,6-TNS in the hydrophobic interior of micelles should result in a substantial decrease in the tumbling motion (rotational velocity) of the probe, as compared to its free, unrestricted motion in a solvent. In fluorescence depolarization spectroscopy experiments this reduced mobility is measured by an increased polarization of luminescence establishing the CMC and monitoring further mobility changes associated with mesophase formation. Fluorescence depolarization of a polymerizable probe 1-PMM was also employed to monitor the formation process of the nanocomposite films. The idea behind using this probe is the possibility of monitoring the polymerization process (i.e., observation of a substantial change in the degree of polarization upon bonding to the inorganic or organic species), in addition to following micelle and lamellar mesophase formation.

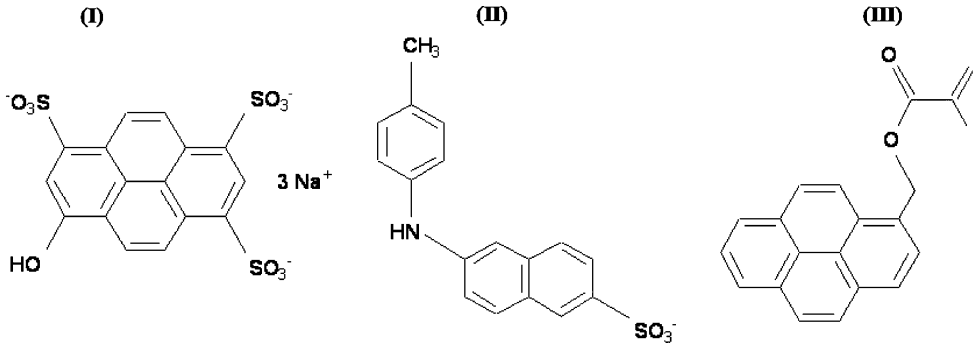

Fig. 1 Molecular structures of the probes pyranine (I), TNS (II), and PMM (III)

2.3 Optical measurements

Fluorescence depolarization measurements, emission spectroscopy, and interferometry are combined to study the dynamic physical and chemical changes that occur as the sol–gel films are deposited on the Si substrates. When the substrate is withdrawn from the solution at a constant rate, a steady-state develops in a few seconds in which the film thickness at a given height above the solution remains constant even though the substrate is moving. The spectroscopic probing of the film formation process is carried out on the dynamic system. Illumination of the film with a monochromatic light causes constructive and destructive interference of light rays reflecting off the top and bottom faces of the film, producing alternating bright bands, and dark bands on the film [36]. Because the film thickness at a given height above the sol level is constant, the interference fringe pattern remains stationary even though the substrate is moving. Film thicknesses can thus be calculated from the fringe patterns.

The experimental setup has been described previously [23]. A mercury lamp filtered to emit 546-nm light was placed at an angle of 65° to the substrate normal to illuminate the film (the angle used in the non-surfactant sol studies). On the other side of the film, a telescopic microscope at an angle of 65° to the substrate normal was used to observe fringes in the film. Interference occurs at thicknesses corresponding to

$$h = \frac{(2m+1)\lambda}{4\left(n^2 - \sin^2\theta_{\mathrm{L}}\right)^{1/2}}, \tag{1}$$

where h is the film thickness, m is the interference fringe number, θ_{L} is the illumination/viewing angle of the interference pattern and n is the refractive index [37]. Based on the measured thickness of the final film, $m = 1$ for the last observable fringe. A slightly different illumination/viewing angle (55°) has been used for the PDM films.

The interference fringes were reproducible under identical withdrawal conditions. When the substrate is withdrawn from the solution at a constant rate, a steady-state develops in a few seconds in which the film thickness at a given height above the solution remains constant even though the substrate is moving. The interference fringes remain constant in the dynamic system. The last observable fringe is called the 0th fringe, or the drying line as used in earlier reports, beyond which the film microstructure evolves more slowly due to continued condensation reactions and equilibration with the overlying atmosphere. The lower fringes are called the first fringe, second fringe, and so on. Continuous solvent evaporation shrinks the film. Each fringe above the sol represents a decrease in the thickness of about 2,800 Å; this value varies with height above the sol because the refractive index increases during processing. For SDS templated films the thickness shrinks to 150 nm from about 3.5 μm near the sol level. In addition to providing a measure of the film thickness, the fringes also serve as a convenient vertical and time scale. Both the time taken and height above the sol level to reach a point on the fringe pattern can be determined. Furthermore changes in thickness correspond directly to volume fraction solvent allowing concentration of non-volatile components to be determined.

Informaiton about the onset and progression of micelle and mesophase formation is established through fluorescence depolarization measurements. The fluorescence depolarization technique uses polarized light to excite a fluorescent and somewhat hydrophobic probe molecule [38]. Probe molecules aligned in the proper orientation will absorb the light and luminesce at a later time, which depends on emission lifetime. Any rotation tumbling of the probe molecules during this time depolarizes the resulting emission. The scrambling of the emission polarization is expressed as P, the degree of polarization:

$$P = \frac{I_{\parallel} - I_{\perp}}{I_{\parallel} + I_{\perp}}, \tag{2}$$

where $I_{\parallel}$ and $I_{\perp}$ are the emission intensities parallel and perpendicular to the polarization of the exciting light. When the probe is free to tumble during the period of the emission lifetime, $I_{\parallel} = I_{\perp}$ and $P = 0$. When the emitter is immobilized, e.g., within the hydrophobic interior of a micelle, or is constrained in its motion, P can have a maximum value of 0.5. This technique, therefore, can

provide information on local structural rigidity and micelle formation.

For all luminescence spectroscopic experiments the excitation source is the 351-nm polarized light from a Coherent Ar^+ laser (50:1 vertical polarization). The laser spot size was focused to about 100 μm permitting excellent spatial resolution. The spot size is smaller than the width of the fringe; changes in adjacent fringes can be easily located. In the fluorescence depolarization experiments, fluorescence of the probe passes through a Glan-Thompson polarizer into a Jarrell-Ash monochromator which was set at the emission maximum of the probe. The slit width varied between 100 and 300 μm, depending on the needs of a particular study. A scrambler was used to offset the polarizing effect from the monochromator. The signal was collected by a photomultiplier (C31034/76, Products for Research), processed by a photon counter (SR400, Stanford Research Systems, Inc.), and displayed on a computer. During the experiment the polarizer was repeatedly rotated to measure $I_{\parallel}$ and then $I_{\perp}$ for about 15 s each (integration time = 0.5 s). The emission spectra were recorded by using an EG&G model 1420 optical multichannel analyzer and a 0.32-m Jobin-Yvon/ISA monochromator for dispersion. The slit width was 200 μm (or 20–50 μm for pyranine experiments in the non-surfactant sol due to the strong signal), and the integration time was 1 s.

3 Results and discussion

A photograph of a characteristic fringe pattern for the non-surfactant sol–gel film as it is withdrawn from the reservoir is shown in Fig. 2. The fringe pattern is stationary and the film thickness at a particular height above the sol level is constant, even though the substrate is constantly moving up.

Probing these dynamic changes is achieved by adding a very low concentration of a suitable luminescent molecular probe to the sol, and taking the emission spectra or polarized emission intensities of the probe at various fringes on the developing film. The combination of interferometry and emission spectroscopy is used to probe the chemical and physical conditions at a particular point during the film development process.

Incorporation of luminescent molecular probes in the films not only allows in situ probing of the film formation process, but also results in luminescent mesostructured thin films. Many other types of molecules can be incorporated and strategies for deliberately placing different molecules in the spatially separated regions have been reported [39–47]. The films are stable at room temperature; they possess the same surface appearance and show the same XRD patterns after months of storage at room temperature.

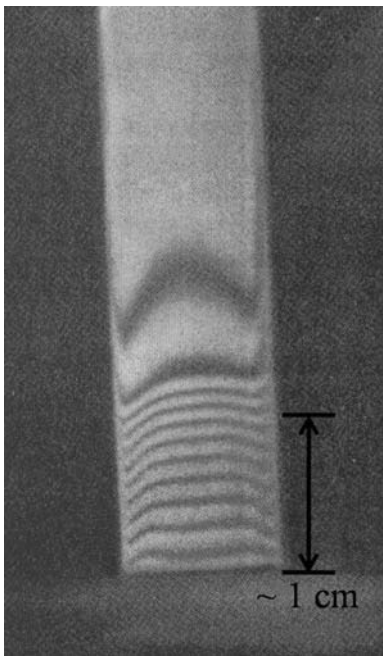

Fig. 2 Photograph of the interference fringe pattern observed on a sol–gel thin film during dip-coating. The substrate is being withdrawn from a sol reservoir and is moving, but the fringe pattern is constant

3.1 CTAB-templated sol–gel silica films

3.1.1 Film structure

Hexagonal mesoporous sol–gel silica films are formed using sols prepared with 2.5 wt% CTAB. At higher CTAB concentrations, other mesophases (lamellar and cubic phases) are formed [19]. The surfactant–silicate interactions leading to the co-assembly of ordered phases have been discussed [48]. The films are uniform in color, and are stable in air. Figure 3a, c show cross-sectional views of the hexagonal phase structure in the 2.5 wt% CTAB-templated sol–gel film and its TEM image [19]. The ordered hexagonal phase is located primarily at the two interfaces between the film and the adjacent support or medium (i.e., the substrate and air). Surface-assisted growth has been reported as important in directing the formation of initial layers of the surfactant array. Additional layers can then build on them into the interior of the film, but the structure-directing effect decreases with distance [8, 10]. XRD patterns of the 2.5 wt% CTAB films (Fig. 4a) show the (100) and (200) peaks with a unit cell constant $a = 42.3$ Å (uncalcined) and $a = 35.3$ Å (calcined). Slightly larger unit cell constants were reported in Martin et al. [12]. The XRD patterns are indicative of a 2-dH mesophase, in which the axes of the pore channels are oriented parallel to the substrate surface. Calcination of the films removes the surfactant, shrinks the pore diameter, and compresses the hexagonal structure. XRD peaks shift to slightly higher 2θ

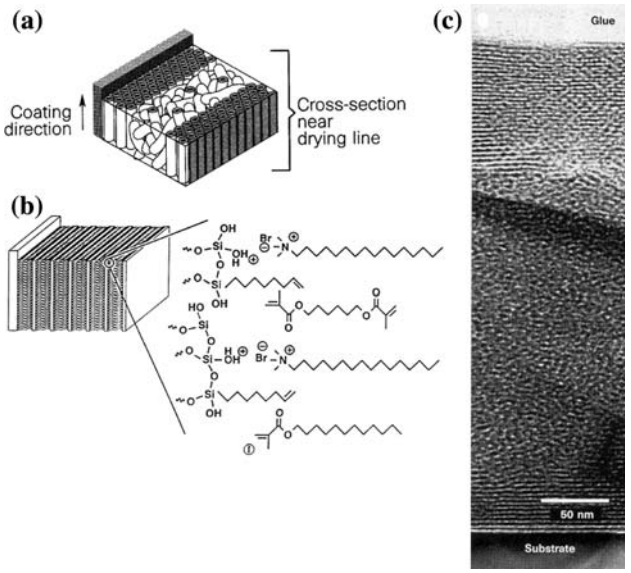

Fig. 3 (**a**) Cross-section of an ordered region of the CTAB-templated sol–gel film near the drying line, depicting the interfacial regions of liquid crystalline order. The hexagonal regions grow from the substrate-film and air-film interfaces toward the film interior. The interior shows a disordered worm-like micellar structure. (**b**) Cross-sectional TEM image of a calcined CTAB-templated 2-D hexagonal sol–gel films. Periodic ordered regions are observed at both the substrate-film and film-vapor (glue) interfaces mainly as brick-like stripes. Brick-like structures presumably result from the constrained 1-D shrinkage of the films upon calcination. (**c**) Cross-sectional view of the nanolaminate construction of the PDM/silica nanocomposite film. The surfactant, monomer, crosslinker, and initiator adjacent to oligomeric silicate surface are shown in this drawing

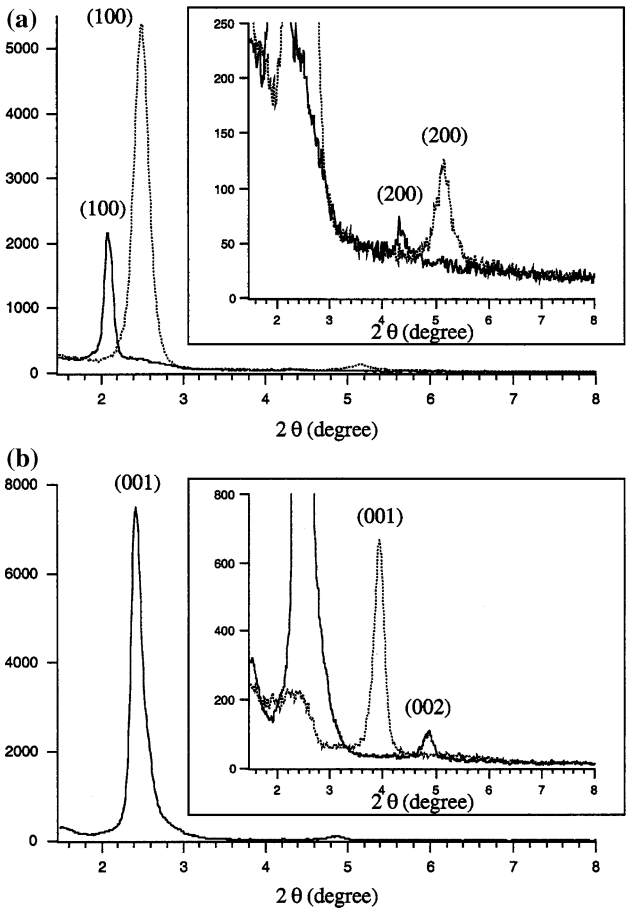

Fig. 4 (**a**) X-ray diffraction patterns of a 2.5-wt% CTAB sol–gel film before and after calcination (*solid trace*—before calcination, *dotted trace*—after calcination). (**b**) XRD patterns of a poly(dodecylmethacrylate)/silica nanocomposite film before and after calcination. The small residual (001) peak observed after calcination indicates that the lamellar phase structure is maintained. A small side peak to the right of the (001) peak is frequently observed, suggesting the presence of a small secondary lamellar structure with a slightly smaller basal spacing

angles. Although it may appear that the peak intensity is higher after calcination, the intensities before and after calcination are sometimes similar.

3.1.2 Monitoring changes in the water content

The dynamic changes in the solvent composition that occur during film formation are monitored by in situ fluorescence spectra of the pyranine probe at various points on the fringe pattern. The variation in the alcohol:water ratio during the film development is monitored by blue (430 nm) to green (510 nm) luminescence band intensity ratios of pyranine [23, 29–32]. In pure alcohol, only the 430 nm band is present. Addition of water to alcohol shows both luminescence bands and the relative band intensities depend on the relative amount of alcohol and water in the solution. In pure water, only the 510 nm peak is observed. The relative intensities of the luminescence bands to the relative percentage of alcohol and water have been calibrated [23]. By measuring the ratio of the two luminescence bands, the percentage of alcohol (or water) in the solution can be determined.

Variation in the water content for the non-surfactant sol–gel films (sol prepared the same way as that used to make the CTAB sol, but without addition of surfactant) has been studied. The water to alcohol ratio increases continuously during film development because of the higher vapor pressure and faster evaporation of alcohol [23]. In the non-surfactant sol, the water content is about 2% and remains low until the final stage of the processing (2nd fringe, 10–11 s), where it reaches about 13%. The water content is between 5 and 7% in the middle period of the processing (3rd to 5th fringe, 8–10 s), and then increases to about 25–30% in the final stage of the film formation process (the region from the 1st fringe to the 0th fringe, 11–13 s). Near the top of the 0th fringe, the water content is close to 40%.

Pyranine has been used to probe changes in the solvent composition during the formation of CTAB-templated

sol–gel silica films, but the results always show that the solvent is still composed of mostly alcohol even in the final stage of the film formation process where preferential alcohol evaporation should result in an enrichment of water content. The water content is 2% at the start of film formation process (11th fringe, 1 s), and then increases to about 11–18% in the middle period of the processing (5th to 7th fringe, 4–5 s). Near the end of the process, the water content is 18% (1st fringe, 7 s). The blue:green intensity ratio dropped to less than 5% at about the end of the processing (0th fringe, 8 s). This is a surprise. A major change in the local environment surrounding the probe molecules may be present.

There are two possibilities that may help explain such changes in the film. At about the end of the film formation process, the CTAB micellar rods have aligned to a hexagonal array and silicate has mostly polymerized to silica. In the previous study, it has been shown that when pyranine adsorbs on the silica surface at the end of the film formation process the luminescence of the probe shifts from predominately the green band to the blue band [23]. Thus one possibility is that it is the probe molecules adsorbing on to the silica surface that causes the drop in the blue:green intensity ratio. Alternatively, it may be the electrostatic interaction or hydrogen bonding between the negatively charged probe and the positively charged surfactant that makes the emission shift to the protonated form. The probe molecules probably reside near the surface of the CTAB micellar rods and do not interact with water to become deprotonated. Pyranine has also been used to study the evolution of solvent composition during formation of negatively charged surfactant SDS (sodium dodecyl sulfate) sol–gel films that form alternating surfactant and silica layered structure [20]. The films are prepared with the same sol composition as the one used in this CTAB film study. The water content increases from 28% at the 1st fringe to 59% at the 0th fringe. The same charges on the probe and SDS should keep the probe from interacting with each other. From these considerations, interaction with the silica wall is less likely the cause for the observed drop in the blue:green intensity ratio, since the SDS film also has silica near the surfactant layers. Electrostatic interaction between the probe and the CTAB micellar rods is a more likely possibility for the observed drop in the intensity ratio. Therefore, while pyranine results show the trend of water enrichment by preferential evaporation of alcohol in the early stages of the processing of the CTAB-templated sol–gel films, pyranine does not accurately report solvent changes near the end of the process.

3.1.3 Monitoring micelle and mesophase formation

To locate the onset of micelle formation and to follow the development of the mesostructure in the film during film deposition, spatially resolved fluorescence depolarization measurements of a hydrophobic dye 2,6-TNS were performed. Figure 5 shows the fluorescence depolarization results of 2,6-TNS during the formation of CTAB-templated sol–gel films.

Within 5 mm above the sol reservoir surface (or 4 s into the dip-coating process), the degree of polarization was close to 0, indicating the probe was freely rotating. At around 6th to 7th fringe, *P*-value abruptly increases to 0.18. This is caused by incorporation of the probe in the hydrophobic micellar interior and indicates that the CMC has been reached. Beyond this point, *P*-values continue to increase, and this change is caused by micelle aggregation and alignment to form micellar rods and eventually the highly-ordered hexagonal phase structure in the films near the end of the film deposition process [19]. Similar *P*-values were measured above the 0th fringe and in the dried film, suggesting that the structure is essentially established as soon as the film is made.

In contrast, *P*-values for the control films with no CTAB added were close to 0 until near the 0th fringe. *P*-values are 0.03 at the 2nd fringe and 0.09 at the 0th fringe. Just above the interference fringe pattern, *P*-value rises to 0.21. The results for the control films are clearly different from those recorded when CTAB is added in the sol. These results provides further evidence that the large increase in the *P*-values during the CTAB film formation process is a result of micelle formation and its transformation to the hexagonal phase structure.

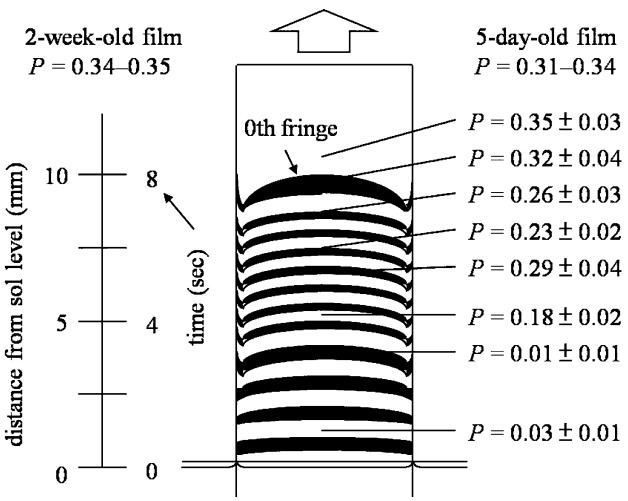

Fig. 5 Schematic diagram of the interferometry and the fluorescence depolarization results of 2,6-TNS during the formation CTAB-templated sol–gel films. The *dark fringes* represent distinctive interference (see Fig. 2). The values of the degree of polarization, *P*, and their standard deviations of the mean are shown to the right of the film

The transformation of CTAB micelles in aqueous solution has been well studied [49–53]. The changes that take place in aqueous solution is similar to the behavior of CTAB observed in the sol–gel films. At very low surfactant concentration, the surfactant is present as free molecules dissolved in the aqueous solution. At slightly higher surfactant concentrations (above 5 wt% CTAB in water and at temperatures above 40°C), the CMC is reached and spherical micelles form [49]. At higher surfactant concentrations (at concentrations between 13 and 35 wt% in water and above 40°C in temperature), spherical micelles coalesce to form elongated cylindrical micelles, also called micellar rods. At still higher concentrations (between 37 and 65 wt% CTAB in water and at temperatures above 45°C), the micellar rods aggregate to form a hexagonal close-packed liquid crystalline array. Finally at very high CTAB concentrations (above 70 wt% CTAB in water and at temperatures above 80°C), the lamellar liquid crystal phase is formed. Lamellar mesophases have been observed in sol–gel films pulled from sols containing 4.2 and 5 wt% CTAB in the sol [19]. CTAB concentrations used in the sol for the mesophase formation in the sol–gel films are much lower than those used in the aqueous solution. Formation of these liquid crystalline phases relies on the solvent evaporation to increase the surfactant concentration in the developing films.

Figure 6 illustrates the surfactant phases to form the hexagonal phase structure driven by solvent evaporation. Although gravitational draining (which does not change the surfactant concentration) is possible, its effect is probably minimal as the stagnation point for this dip-coating regime is near the reservoir surface.

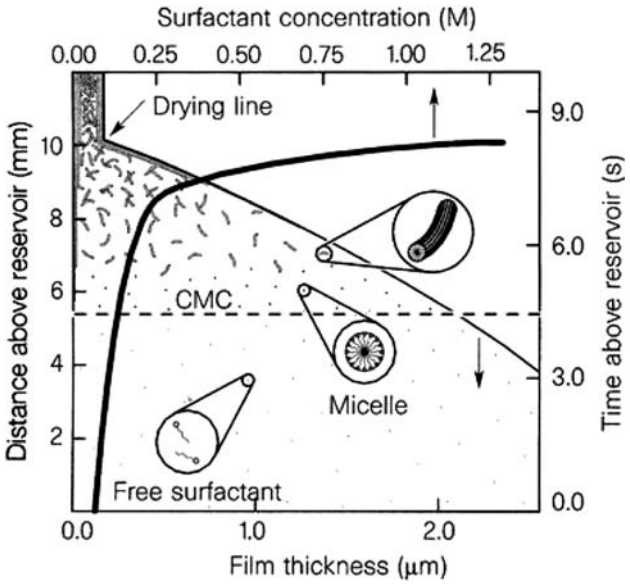

Fig. 6 Schematic diagram of the steady-state film profile showing the locations of the stages of surfactant phases leading to the final hexagonal phase structure. The film-thickness profile was calculated from the interference pattern assuming a linear refractive index gradient from 1.25 at the liquid meniscus to 1.35 at the drying line (0th fringe). Also shown are the distance and time above the sol reservoir and the surfactant concentration. The surfactant concentration was calculated from the thickness profile assuming no surfactant volatility

3.2 Organic–inorganic poly(dodecylmethacrylate)/silica nanocomposite films

3.2.1 Film structure

The organic–inorganic PDM/silica nanocomposite films were developed to mimic seashell architectures which comprise organic and inorganic layers and exhibit enhanced hardness and toughness [28]. The formation mechanism has been proposed [28]. During dip-coating, continuous evaporation of solvent promotes cooperative assembly of the surfactant-monomer micellar species and the silica precursor into an interfacially organized liquid-crystalline mesophase with alternating inorganic and organic layers. Thermal or photo-initiation causes organic polymerization to occur in the film after film formation. Combining the organic polymerization with further inorganic polymerization in the post-film formation treatment, the inorganic and organic layers then lock-in the laminated architecture and covalently bond the organic–inorganic interface. Figure 3c shows the nanolaminate construction of PDM/silica nanocomposite films [28].

The laminated structure and the extent of polymerization of the final films were characterized by XRD patterns, Fourier-transform infrared spectroscopy, magic-angle-spinning solid-state NMR, and TEM [28]. Figure 4b shows the XRD pattern of a PDM/silica nanocomposite film before (as-deposited, not irradiated with UV lamp to polymerize the organic species) and after calcination. These XRD patterns are consistent with a (001)-lamellar phase with basal spacing $c = 36.4$ Å. The small residual peak observed in the calcined XRD pattern suggests that the lamellar mesostructure is maintained [28]. The basal spacing after calcination is 22.4 Å. Slightly smaller basal spacing values were reported in Sellinger et al. [28].

3.2.2 Monitoring micelle and mesophase formation

To monitor the formation process of the nanocomposite films, fluorescence depolarization of a polymerizable probe 1-PMM was employed. The fluorescence depolarization results of the PDM/silica nanocomposite films, made from a sol containing all the species (i.e., 3.5 wt% CTAB, organic monomer, crosslinker, photo-initiator, and the unsaturated alkyltrialkoxysilane coupling agent), are shown in Fig. 7.

For the control experiments, fluorescence depolarization measurements of films formed from a sol containing 3.5 wt% CTAB in the sol + the coupling agent (7-OTS) were made. These control films show excellent XRD patterns consistent with the lamellar mesophase structure. Films made with another sol containing 3.5 wt% CTAB only show little or no ordered structure according to the XRD patterns; these results will be discussed later.

The fluorescence depolarization results for the sol containing all the components are discussed first. In the early and middle periods of the processing, *P*-values remain low. In this period probe molecules are surrounded by the organic species or the derivatized silicate. A small amount of the probe may be bonded to these species, but there is a sufficient amount of solvent present in the film to allow free rotational mobility of the free and bonded probes. *P*-values increase to 0.10 around the 3rd fringe and continue to increase to 0.26 at the 0th fringe. The CMC is exceeded around this point (9–10 s into the dip-coating process), and the micelle continues to aggregate and transform through the extremely wide 0th fringe into a highly ordered organic–inorganic lamellar structure. The final lamellar structure is established around the upper edge of the 0th fringe. It has been shown that the lamellar phase begins with the formation of a monolayer on the substrate and subsequent layers grow on top of this initial layer [28]. Formation of this monolayer may occur soon after the CMC is exceeded. The striking feature of this fringe pattern is the especially wide and gradually fading 0th fringe. It is possible that this broad fringe is a result of a prolonged long-range structural organization period; the greater

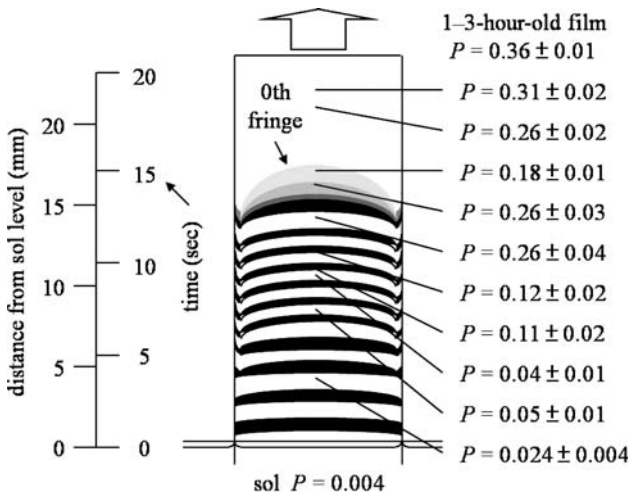

Fig. 7 Schematic diagram of the interferometry and the fluorescence depolarization results of 1-PMM during the formation of organic–inorganic PDM/silica nanocomposite films. The values of the degree of polarization, *P*, and their standard deviations of the mean are shown to the right of the film

complexity and rigidity of this final structure slows down the drying process.

Since laser irradiation during the in situ fluorescence depolarization measurements can also cause polymerization of the organic species and the probe in the region of the laser spot, the *P*-values recorded may also include contributions from the polymerization reaction. For example, the high *P*-values measured in the upper fringes may be indicative of bonding of the probe to organic species. Our experiments, however, can not distinguish the contribution to the fluorescence polarization of the incorporation of probe in the micellar interior from that of the polymerization-induced decrease of probe motion.

The sol containing 3.5 wt% CTAB and the coupling agent OTS (no monomer DM and crosslinker HDM) shows an exceptionally highly-ordered lamellar-phase structure, evidenced by the strong and sharp XRD peaks. The added coupling agent evidently plays an important role in directing this highly-ordered structure in the film. This sol can be compared to the sol containing all the components to see how the micelle to lamellar phase transformation behaves in the absence of the polymerizable organic species.

The fluorescence depolarization results for the sol, containing 3.5 wt% CTAB and the coupling agent OTS, show that the CMC is exceeded around the 6th fringe (6–7 s into the dip-coating process), and the micelles then disrupt at the 4th fringe (8 s into the dip-coating process) and reorganize into the final lamellar mesophase at the 0th fringe. As the solvent continues to evaporate and the surfactant concentration continues to increase, the probe that is initially incorporated in the micellar interior becomes re-exposed to the solvent and increases its rotational mobility. As the micelles reorganize into the more energetically favorable lamellar phase structure [49–53], the probe mobility once again is hindered. *P*-values thus decrease from 0.10 to 0.11 in the 5th to 6th fringe region to around 0.01–0.06 in the 2nd to 4th fringe region and then back up to 0.20 at the 0th fringe. This behavior is clearly different from that observed in the films made from the sol containing all of the components, where a continuous increase in the degree of polarization was measured. The added polymerizable organic species in the sol may significantly reduce the probe mobility once micelle is formed, due to the subsequent alignment of the organic species with surfactant to form the lamellar structure. When the sol does not contain those organic species, probe mobility is enhanced when the probe becomes re-exposed to the solvent after micelle disruption. The final structure is essentially established above the 0th fringe, although residual probe motion may still be present for several seconds. The *P*-values recorded within the first few seconds after film formation range from 0.16 to 0.32. The *P*-value for 1-week-old films is 0.21–0.31, and 0.25–0.26

for 1-month-old films. It is not clear why larger *P*-values (above 0.30) were not observed in dried films from this system, but it could be reflective of the lower dimensional constraint in the lamellar system.

In the case of the sol containing only CTAB in the sol, the XRD patterns indicate that the films possess little or no ordered structure. The results suggest that at a film pulling speed of 6.9 cm/min, surfactant molecules in this system do not have enough driving force to effectively assemble into an ordered structure, even though the CTAB concentration in the sol is high. A separate film-pulling experiment using the same sol, but at higher pulling speed ($\sim$15.7 cm/min), does show good XRD patterns that indicate hexagonal phase structure in the films. The fluorescence depolarization results for this sol are consistent with the observation of little or no ordered structure in the films; *P*-values are close to 0 until the 0th fringe, and increases to 0.15–0.25 in the region above the fringe pattern. Nine-day-old films give a *P*-value of 0.31. The results are similar to those obtained in a separate pure silica film study. The films made from this sol show that the probe experiences approximately the same degree of mobility both in the presence and absence of a large amount of surfactant in the sol if the surfactant molecules do not organize into an ordered mesophase.

4 Summary

Surfactant-templated mesostructured sol–gel thin films formed by the rapid dip-coating method can possess highly-ordered hexagonal, lamellar, and cubic structures. The dynamic chemical and structural changes occurring during the pure and mesostructured sol–gel film formation can be conveniently studied by the use of incorporated luminescent probes. By taking luminescence spectra of the probes at various points on the interference fringe pattern of a developing film, these changes can be followed. It should be noted that incorporation of luminescent dyes to the films not only allows detection of the processes involved to form these highly-ordered mesostructured sol–gel films, but also is a synthetic method for making luminescent mesostructured materials.

In this study CTAB-templated sol–gel films give a hexagonal phase structure at the surfactant concentration used (2.5 wt% of sol). Organic–inorganic PDM/silica nanocomposite films show lamellar phase structure. XRD patterns and TEM images of these films confirm the existence of these ordered structures. These films are stable for a long period of time.

Pyranine was used to follow the evolution of solvent composition for the CTAB-templated sol–gel films and the non-surfactant sol–gel films. The trend of increased water content by preferential evaporation of alcohol has been observed and quantified in both cases. Possible electrostatic interaction between the probe and the CTAB micellar rods near the end of the film formation process interferes with the accurate report of the solvent changes.

2,6-TNS was used to follow the micelle and the hexagonal phase formation for the CTAB-templated sol–gel films by measurements of its fluorescence depolarization. Micelles form at about the mid-point in the film formation process, and continuously assemble into the micellar rods and then the hexagonal phase structure in the films. The ordered hexagonal structure is mainly observed at the two interfaces of the film by a surface-assisted mechanism.

In the case of the PDM/silica nanocomposite films, fluorescence depolarization measurements of a polymerizable probe 1-PMM was used to locate the micelle formation. The results suggest that more time is required for the organic species added to co-assemble with the silicate and surfactant molecules into the highly-ordered lamellar structure, giving an unusually broad 0th fringe. The presence of polymerizable organic species reduces the rotational mobility of the probe after the micelle forms. This is indicated by a continuous increase in the values of the degree of polarization after the CMC is exceeded. For films made from a sol containing only CTAB and the coupling agent OTS, the results show micelle formation, followed by disruption and reorganization of the micelle to form films with a highly-ordered lamellar mesophase. For films pulled from a sol containing only CTAB in the sol, little or no ordered structure is observed, presumably because of the slow film pulling speed used. At a higher pulling speed, hexagonal phase films were made. The fluorescence depolarization measurements indicate unhindered probe motion throughout the entire film development due to randomly ordered surfactant in the films.

The combination of the in–situ luminescence studies of the films as they form with the characterizations of the final dried films by XRD patterns and TEM images makes possible a more complete understanding of the processes that occur during the dip-coating process that lead to mesostructured materials. This understanding can assist in the design of mesostructured sol–gel films in the future with desired structures and properties, and lead to the realization of possible applications.

Acknowledgement This work was made possible by grants from the National Science Foundation (Grant DMR0346610 and CHE 0507929).

References

1. Dunn B, Zink JI (2007) Acc Chem Res 40:747
2. Soler-Illia GJAA, Sanchez C, Lebeau B, Patarin J (2002) Chem Rev 102:4093

3. Loy DA, Shea KJ (1995) Chem Rev 95:1431
4. Brinker CJ, Scherer GW (1990) Sol–gel science. Academic, San Diego
5. Kresge CT, Leonowicz ME, Roth WJ, Vartuli JC, Beck JS (1992) Nature 359:710
6. Beck JS, Vartuli JC, Roth WJ, Leonowicz ME, Kresge CT, Schumitt KD, Chu CTW, Olson DH, Sheppard EW, McCullen SB, Higgins JB, Schlenker JL (1992) J Am Chem Soc 114:10834
7. Ogawa M (1994) J Am Chem Soc 116:7941
8. Yang H, Kuperman A, Coombs N, Maniche-Afara S, Ozin GA (1996) Nature 379:703
9. Yang H, Combs N, Sokolov I, Ozin GA (1996) Nature 381:589
10. Aksay IA, Trau M, Manne S, Honma I, Yao N, Zhou L, Fenter P, Eisenberger PM, Gruner SM (1996) Science 273:892
11. Tolbert SH, Schäffer TE, Feng J, Hansma PK, Stucky GD (1997) Chem Mater 9:1962
12. Martin JE, Anderson MT, Odinek J, Newcomer P (1997) Langmuir 13:4133
13. Ryoo R, Ko CH, Cho SJ, Kim JM (1997) J Phys Chem B 101:10610
14. Sanchez C, Boissiere C, Grosso D, Laberty C, Nicole L (2007) Chem Mater 20:682
15. Ogawa M, Kikuchi T (1998) Adv Mater 10:1077
16. Tate MP, Eggiman BW, Kowalski JD, Hillhouse HW (2005) Langmuir 21:10112
17. Grosso D, Cagnol F, Soler-Illia GJAA, Crepaldi EL, Amenitsch H, Brunet-Bruneau A, Bourgeois A, Sanchez C (2004) Adv Funct Mater 14:309
18. Nicole L, Boissière C, Grosso D, Quach A, Sanchez C (2005) J Mater Chem 15:3598
19. Lu Y, Ganguli R, Drewien CA, Anderson MT, Brinker CJ, Gong W, Guo Y, Soyez H, Dunn B, Huang MH, Zink JI (1997) Nature 389:364
20. Huang MH, Dunn BS, Soyez H, Zink JI (1998) Langmuir 14:7331
21. Huang MH, Dunn BS, Zink JI (2000) J Am Chem Soc 122:3739
22. Grosso D, Babonneau F, Sanchez C, Soler-Illia GJAA, Crepaldi EL, Albouy PA, Amenitsch H, Balkenende AR, Brunet-Bruneau A (2003) J Sol Gel Sci Technol 26:561
23. Nishida F, McKiernan JM, Dunn B, Zink JI, Brinker CJ, Hurd AJ (1995) J Am Chem Soc 78:1640
24. Franville AC, Dunn B, Zink JI (2001) J Phys Chem B 105:10335
25. Lan EH, Dunn B, Zink JI (2000) Chem Mater 12:1874
26. Huang MH, Soyez H, Dunn BS, Zink JI (2000) Chem Mater 12:231
27. Huang MH, Kartono F, Dunn B, Zink JI (2002) Chem Mater 14:5153
28. Sellinger A, Weiss PM, Nguyen A, Lu Y, Assink RA, Gong W, Brinker CJ (1998) Nature 394:256
29. Clement NR, Gould M (1981) Biochemistry 20:1534
30. Kaufman VR, Avnir D, Pines-Rojanski D, Huppert D (1988) J Non Cryst Solids 99:379
31. Dunn B, Zink JI (1997) Chem Mater 9:2280
32. Wolfbeis OS, Fürlinger E, Kroneis H, Marsoner H (1983) Fresnius Z Anal Chem 314:119
33. Kano K, Fendler JH (1978) Biochim Biophys Acta 509:289
34. Pouxviel JC, Dunn B, Zink JI (1989) J Phys Chem 93:2134
35. Edelman GM, McClure WO (1968) Acc Chem Res 1:65
36. Serway RA, Faughn JS (1992) College physics. Saunders College Publishing, New York, pp 817
37. Ditchurn RW (1976) Light, 3rd edn. Academic, London, pp 113
38. Weber G (1966) In: Hercules DM (ed) Fluorescence and phosphorescence analysis. Interscience, New York, pp 217–224
39. Miller JM, Dunn B, Valentine JS, Zink JI (1996) J Non Cryst Solids 202:279
40. Dave BC, Miller JM, Dunn B, Valentine JS, Zink JI (1997) J Sol Gel Sci Technol 8:629
41. Chia S, Jun U, Tamanoi F, Dunn BS, Zink JI (2000) J Am Chem Soc 122:6488
42. Corriu RJP, Mehdi A, Reye C (2005) J Mater Chem 15:4285
43. Corriu RJP, Mehdi A, Reye C, Thieuleux C (2002) Chem Commun 1382
44. Hernandez R, Franville AC, Minoofar P, Dunn B, Zink JI (2001) J Am Chem Soc 123:1248
45. Minoofar PM, Hernandez R, Franville AC, Chia S, Dunn B, Zink JI (2003) J Sol Gel Sci Technol 26:571
46. Minoofar PM, Dunn BS, Zink JI (2005) J Am Chem Soc 127:2656
47. Johansson E, Zink JI (2007) J Am Chem Soc 129:14437
48. Huo Q, Margolese DI, Ciesla U, Demuth DG, Feng P, Gier TE, Sieger P, Firouzi A, Chmelka BF, Schüth F, Stucky GD (1994) Chem Mater 6:1176
49. Raman NK, Anderson MT, Brinker CJ (1996) Chem Mater 8:1682
50. Ross S, Morrison ID (1988) Colloid systems and interfaces. Wiley, New York, p 173
51. Myers D (1988) Surfactant science and technology. VCH Publishers, New York, p 81
52. Clint JH (1992) Surfactant aggregation. Chapman & Hall, New York, p 147
53. Rosen MJ (1989) Surfactants and interfacial phenomena, 2nd edn. Wiley, New York, p 108